Open Access

OBM Neurobiology

LIDSEN Publishing Inc.

Short Communication

Targeted MRI (tMRI) of Small Increases in the T_1 of Normal Appearing White Matter in Mild Traumatic Brain Injury (mTBI) Using a Divided Subtracted Inversion Recovery (dSIR) Sequence

Gil Newburn [1], Joshua P McGeown [1, 2], Eryn E Kwon [1, 2, 3], Maryam Tayebi [1, 2], Paul Condron [1, 2], Taylor Emsden [1], Samantha J Holdsworth [1, 2], Daniel M Cornfeld [1, 2], Graeme M Bydder [1, 4, *]

1. Mātai Medical Research Institute, Tairāwhiti-Gisborne, New Zealand; E-Mails: Gil@Neuropsychiatrygilnewburn.co.nz; j.mcgeown@matai.org.nz; e.kwon@matai.org.nz; m.tayebi@matai.org.nz; p.condron@matai.org.nz; t.emsden@matai.org.nz; s.holdsworth@matai.org.nz; d.cornfeld@matai.org.nz; gbydder@health.ucsd.edu
2. Department of Anatomy & Medical Imaging, Faculty of Medical and Health Sciences & Centre for Brain Research, University of Auckland, New Zealand
3. Auckland Bioengineering Institute, Auckland, New Zealand
4. Department of Radiology, University of California San Diego, San Diego, CA, USA

* **Correspondence:** Graeme M Bydder; E-Mail: gbydder@health.ucsd.edu

Academic Editor: Yasushi Shibata

Special Issue: Neuroimaging of Traumatic Brain Injury

OBM Neurobiology
2023, volume 7, issue 4
doi:10.21926/obm.neurobiol.2304201

Received: June 30, 2023
Accepted: December 12, 2023
Published: December 14, 2023

Abstract

In modelling studies targeted MRI (tMRI) of small increases in the T_1 of tissues using divided Subtracted Inversion Recovery (dSIR) sequences show ten or more times the contrast seen with conventional IR sequences. This may be particularly useful in imaging normal appearing white matter where there may be small changes in T_1 and/or T_2 in disease but these changes may be insufficient to produce useful contrast with conventional T_2-weighted spin echo (T_2-wSE) and T_2-FLuid Attenuated Inversion Recovery (T_2-FLAIR) sequences. In a case of recurrent mild Traumatic Brain Injury (mTBI), very extensive high contrast abnormalities were seen in white matter using a dSIR sequence that targeted small increases in T_1 in areas where no

abnormality was apparent with T_2-wSE or T_2-FLAIR sequences. The increases in T_1 may be due to neuroinflammation and/or degeneration which produces the abnormalities seen on the dSIR images. tMRI of normal appearing white matter may have widespread application in clinical MRI of the brain.

Keywords
Targeted magnetic resonance imaging (tMRI); divided subtracted inversion recovery (dSIR); normal appearing white matter; mild traumatic brain injury; neuroinflammation; neurodegeneration

1. Introduction

It is estimated that nearly half of the World's population will experience one or more Traumatic Brain Injuries (TBIs) during their lifetimes [1]. While Magnetic Resonance Imaging (MRI) has a significant role in the diagnosis and management of TBI, there is pathological evidence of neuroinflammation in the brain in TBI that may not be apparent with conventional sequences such as Magnetization Prepared Rapid-Acquisition Gradient Echo (MP-RAGE), T_2-weighted spin echo (T_2-wSE) and T_2-FLuid Attenuated Inversion Recovery (T_2-FLAIR) sequences [2-4]. It is possible that neuroinflammation may cause small increases in T_1 and/or T_2, but that conventional sequences are not sensitive enough to produce recognizable contrast from these changes. To address this problem we implemented a divided Subtracted Inversion Recovery (dSIR) sequence targeted at small increases in T_1 due to disease in white matter. In modelling studies, dSIR sequences can increase the sensitivity of MRI to small changes in T_1 in the brain by ten or more times [5]. Consequently these sequences could reveal abnormalities which are not apparent with conventional sequences.

In this paper we describe the theory underlying the use of dSIR sequences and illustrate their use in a case of recurrent mild TBI (mTBI).

2. Theory

2.1 The dSIR T_1-filter

The long repetition time (TR) inversion recovery (IR) sequence has a T_1 segment for which the signal S_{T_1} is given by:

$$S_{T_1} = \left(1 - 2e^{-TI/T_1}\right) \quad (1)$$

where TI is the inversion time (fixed for a given IR sequence) and T_1 is the longitudinal relaxation time of different tissues. This function is described as a T_1-filter and is shown in phase-sensitive (ps) reconstructed form in Figure 1A where it has the features of a low pass filter (i.e., it passes low values of T_1, which take positive filter values, and blocks or opposes higher values of T_1 which take negative filter values), and in magnitude (m) reconstructed form in Figure 1B where it has the features of a notch filter. It permits the passage of T_1 values that are lower or higher than those within the notch region while attenuating or blocking T_1 values within the notch itself.

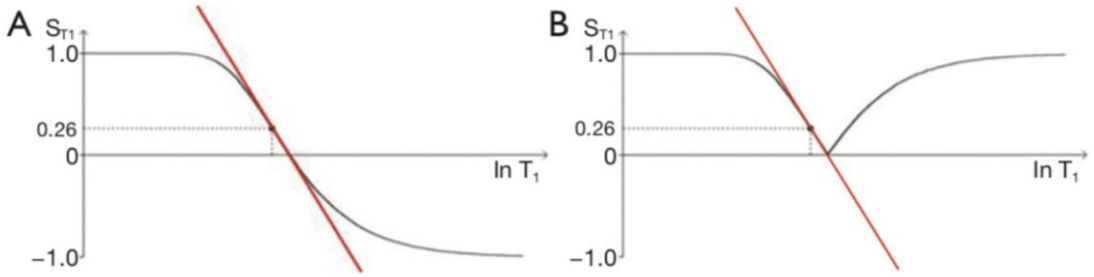

Figure 1 IR T_1-filters with phase-sensitive (ps) (A) and magnitude (m) reconstruction (B) using logarithmic (ln T_1) X axes. (A) is a low pass T_1-filter and (B) is a notch T_1-filter. (A) shows both positive and negative values for S_{T1} whereas (B) shows negative values "reflected" across the X axis so that they become positive. The maximum slopes of the T_1-filters are shown as red lines, and are negative in both cases. They are achieved at 0.26 of the maximum value of the two T_1-filters.

Figure 2A (left) shows an IR m (notch) T_1-filter with a short TI_s (e.g., the Short TI IR or STIR sequence) for the brain where gray matter (G) has a higher signal than white matter (W). The slope of the filter between W and G is strongly positive. An increase in T_1 (positive longitudinal green arrow, ΔT_1) along the ln X axis is multiplied by the positive slope of the filter (red line) to give the resulting positive change in signal or contrast ΔS (positive vertical blue arrow) using the small change approximation of differential calculus.

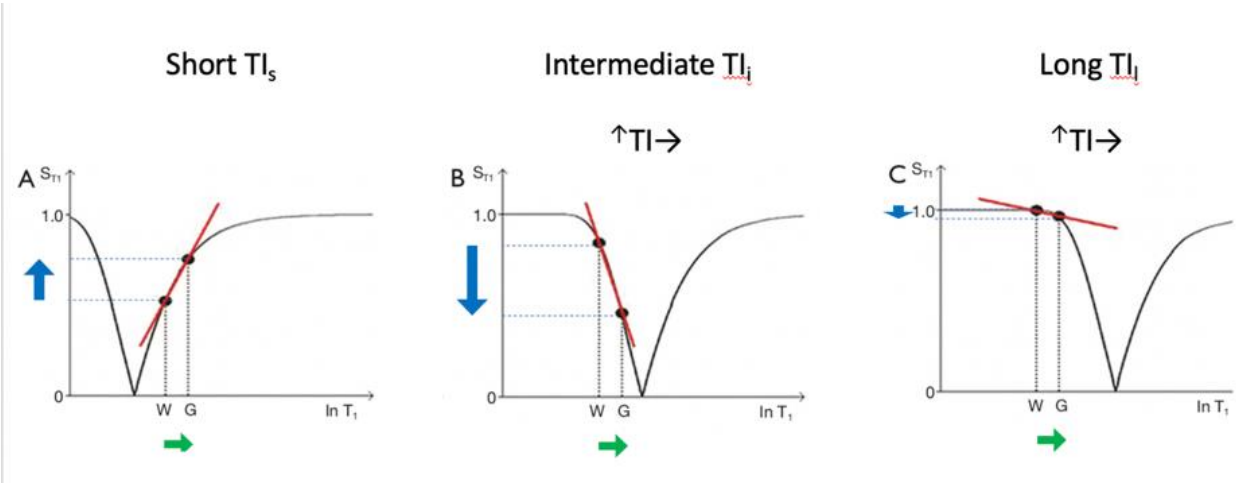

Figure 2 The long TR IR sequence. T_1-filters for short TI_s (A, left), intermediate TI_i (B, center) and long TI_l (C, right) values using logarithmic (ln T_1) X axes. The positions of white (W) and gray (G) matter are the same at each TI. TI is increased from TI_s (left) to TI_i (center) and increased further to TI_l (right). The increase in T_1 from W to G (horizontal green arrows ΔT_1) is multiplied by the relevant slopes of the T_1-filters (red lines) and produces strongly positive, strongly negative, and mildly negative contrast in (A), (B) and (C) respectively (vertical blue arrows), as TI is increased from left to right.

When TI is increased to an intermediate TI_i as in Figure 2B (center) the T_1-filter is shifted to the right. W and G are fixed in the same position on the ln X axis, and W now has a higher signal than

G. The same increase in T_1 as in Figure 2A (positive horizontal green arrow, ΔT_1) is multiplied by the negative slope of the T_1-filter and this produces a negative change in signal or contrast ΔS (negative vertical blue arrow).

When TI_i is increased further to a long TI_i, the T_1-filter is displaced further to the right, as in Figure 2C (right). W has a slightly higher signal than G, and the slope of the T_1-filter between them is negative but of smaller size than in Figure 2B. The same increase in T_1 as in Figures 2A and 2B (positive horizontal green arrow, ΔT_1) is multiplied by the slightly negative slope of the T_1-filter (less negative than in Figure 2B) and produces a small negative difference in signal or contrast ΔS which is less in size than that in Figure 2B (negative vertical blue arrows). The sequence weighting of the T_1-filter, which is the slope or first partial derivative of the T_1-filter, is highly positive in (Figure 2A), highly negative in (Figure 2B) and slightly negative in (Figure 2C) using a short TI_s, an intermediate TI_i and a long TI_l, respectively.

Two m IR T_1-filters with different TIs (TIshort, TI_s and TIintermediate, TI_i) are shown in Figure 3A. They are subtracted to give the Subtracted IR (SIR) T_1-filter in Figure 3B. The SIR T_1-filter is steep in the X axis region between the T_1s corresponding to the two nulling TIs of the T_1-filters shown in Figure 3A, i.e., in the middle Domain (mD). In the mD, the negative slope of the TI_i is subtracted from the positive slope of TI_i to nearly double the slope of the SIR T_1-filter. The width of the mD is determined by the difference in TI between the TI_s and TI_i T_1-filters, ΔTI. Small ΔTIs give a narrow mD and large ΔTIs give a wide mD.

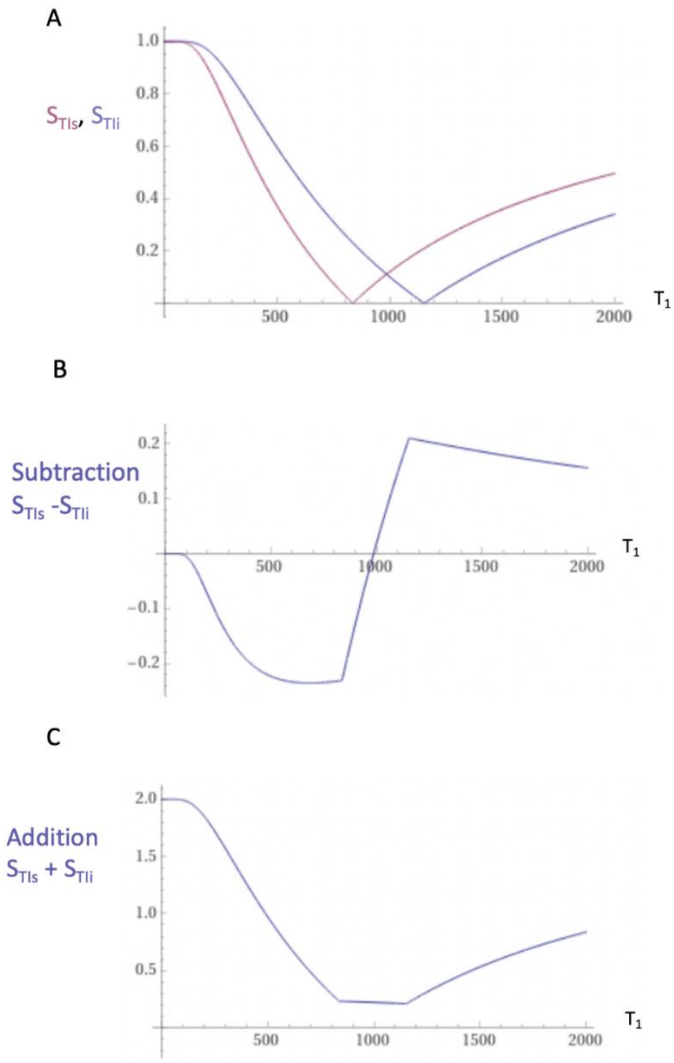

Figure 3 Subtracted IR (SIR) and Added IR (AIR) T_1-filters. T_1 is shown along the linear X axes and is in ms. (A) shows the TI_s T_1-filter (pink) and TI_i T_1-filter (blue), (B) shows the subtraction (S_{TIs} - S_{TIi}) IR or SIR T_1-filter, and (C) shows the addition (S_{TIs} + S_{TIi}) IR or AIR T_1-filter. In (B) the slope of the curve in the mD in the SIR T_1-filter is about double that of the S_{TIs} filter (pink in [A]). In (C) the signal at T_1 = 0 is doubled to 2.0, and the signal in the mD is reduced to about 0.20 in the nearly linear, slightly downward sloping central part of the AIR T_1-filter (i.e. in the middle Domain, mD).

The two T_1-filters in Figure 3A can also be added as an Added IR (AIR) T_1-filter which is shown in Figure 3C. Within the mD in the AIR T_1-filter there is a low signal with a nearly linear slightly downward sloping curve.

Figure 4A shows the divided subtracted IR (dSIR) T_1-filter in which the SIR T_1-filter in Figure 2B is divided by the AIR T_1-filter in Figure 2C. It has a bipolar form. The dSIR T_1-bipolar filter shows a very nearly linear highly positive slope in its mD. In the mD, the SIR T_1-filter is divided by the fraction sized AIR T_1-filter and this increases its slope.

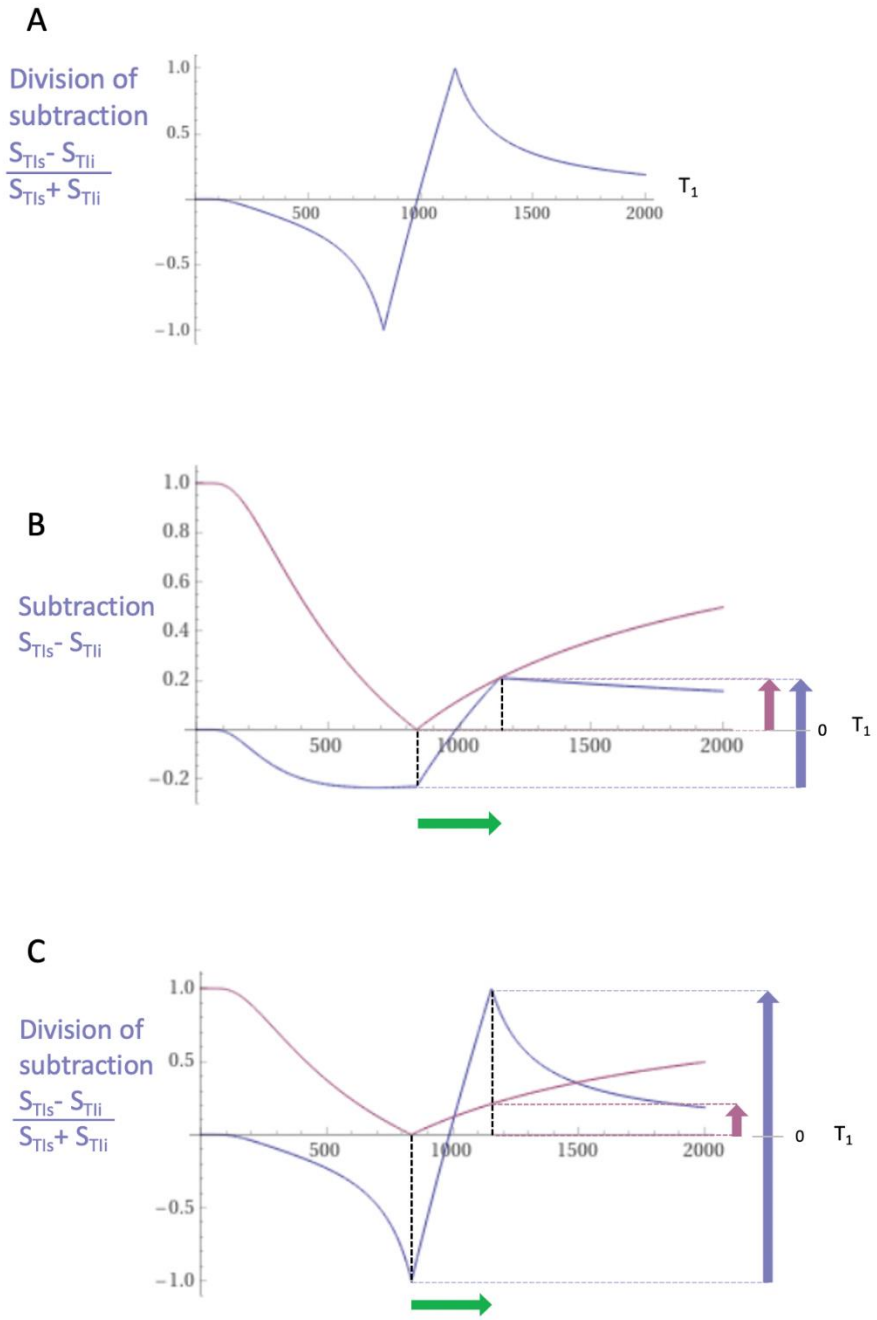

Figure 4 (A) shows division (d) of the subtraction (S_{TIs} - S_{TIi}) T_1-filter (Figure 3B) by the addition (S_{TIs} + S_{TIi}) T_1-filter to give (S_{TIs} - S_{TIi})/(S_{TIs} + S_{TIi}) or SIR/AIR = dSIR T_1-filter. This has a bipolar form. The X axes are linear and are in ms. (B) shows a comparison of the conventional IR S_{TIs} T_1-filter (pink) and the subtraction SIR T_1-filter (blue) for a small increase in T_1 (positive horizontal green arrow, ΔT_1). (C) is a comparison of the S_{TIs} T_1-filter (pink) with the dSIR T_1-filter (blue) for a small increase in T_1 (positive horizontal green arrow, ΔT_1). In (B), the increase in signal (i.e., contrast) with the T_1-SIR filter is about twice that of the conventional IR T_1-filter (right vertical blue and pink arrows). In (C) the increase in contrast of the dSIR T_1-bipolar filter is ten or more times greater than that of the conventional IR T_1-filter (right vertical blue and pink arrows).

Figure 4B compares the contrast (difference in signal) from the short TI T_1-filter, S_{TIs} (pink) which is that of a conventional IR sequence such as MP-RAGE, to that from a SIR T_1-filter (blue). For the same increase in T_1 in disease (positive horizontal green arrow in the mD, ΔT_1) the positive vertical arrows on the right show that the contrast produced by the SIR T_1-filter (blue) is at least double that produced by the S_{TIs} filter (pink).

Figure 4C compares the contrast produced by the short TI T_1-filter, S_{TIs} (pink) to that from a dSIR T_1-bipolar filter (blue). For the same increase in T_1 (positive horizontal green arrow, ΔT_1) the dSIR T_1-bipolar filter generates about ten times more contrast (vertical blue arrow on the right) than that produced by the S_{TIs} T_1-filter (vertical pink arrow on right).

For imaging small increases in T_1 from normal in white matter, the narrow mD dSIR T_1-bipolar filter is targeted at nulling normal white matter using TIs, as well as detecting the small increases in T_1 in disease by using a slightly longer second TI, TI_i.

With the dSIR sequence, as ΔT_1 is decreased, the second TI can be moved closer to the first TI to match this change, and so the slope of the T_1-bipolar filter in the mD becomes steeper. As a result, as ΔT_1 decreases, the amplification produced by the sequence is increased to compensate, and the contrast in the mD is maintained. This continues up until the point where the image becomes noise and/or artefact limited. It is of particular value in imaging contrast produced by small changes in ΔT_1.

2.2 Contrast at Tissue Boundaries

At a boundary between two pure tissues, (such as white and gray matter) the T_1s of voxels with mixtures of the two tissues within them typically span the range of T_1 values between those of the two pure tissues. If a narrow mD dSIR T_1-bipolar filter (e.g., with TI_s nulling normal white matter, and TI_i longer than TI_s but less than that needed to null gray matter) is used, a T_1 value between those of the two pure tissues can result in a high signal $S_{W,G}$, for a value of T_1 between those of white and gray matter as in Figure 5. This high signal is seen at the boundary between white and gray matter and is on subsequent images (e.g. Figure 6, left column). High signal boundaries between white and gray matter on narrow mD dSIR images are a unique feature of this type of imaging.

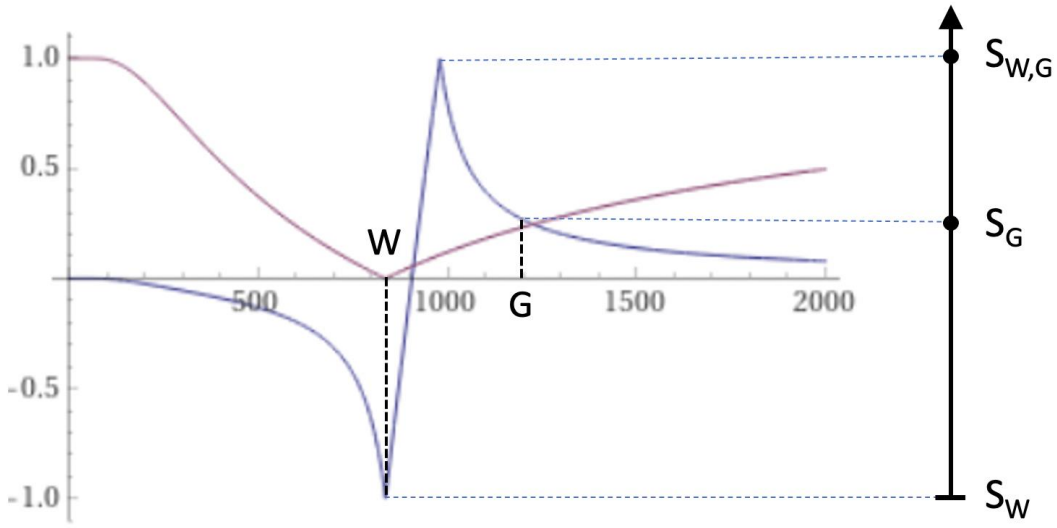

Figure 5 This shows a narrow mD dSIR T_1-bipolar filter with a mD extending from white matter (W) to a $T_{1W,G}$ between the TIs of W and gray matter (G) (blue), and a white matter nulled conventional IR T_1-filter e.g. MP-RAGE (pink). The X axis is linear and is shown in ms. The peak signal ($S_{W,G}$) appears between W and G along the X axis where there is a partial volume effect between W and G producing a $T_{1W,G}$ between the T_1s of W and G. This results in the high signal, $S_{W,G}$ between W and G. This corresponds to the high signal boundary between W and G shown in the following Figure 6 (left column).

2.3 T_1 Maps

To better understand the T_1-bipolar filter, a linear equation of the form y = mx + c can be used to approximate the filter in the mD. The equation is produced by fitting a straight line between the first and last points of the mD (i.e. first point x = TI_s/ln 2 and y = -1, and last point x = TI_i/ln 2 and y = +1). In the mD, S_{dSIR} is then given by:

$$S_{dSIR} \approx \frac{\ln 4}{\Delta TI} T_1 - \frac{\Sigma TI}{\Delta TI} \quad (2)$$

where ΔTI = TI_i - TI_s (i.e., second TI minus first TI) which is positive, and ΣTI = TI_s + TI_i. Note that because ΔTI is positive, the slope $\frac{\ln 4}{\Delta TI}$ is positive (e.g., Figures 4A, 4C and 5), and the offset is negative.

The expression in Eq. (2) captures four key features of the dSIR T_1-bipolar filter, firstly, the near linear change in signal with T_1 in the mD, secondly, the filter has a slope equal to ln 4/ΔTI, thirdly the filter shows high sensitivity to small changes in T_1 when the size of ΔTI is small. As the size of ΔT_1 is decreased, if the magnitude of ΔTI is decreased to match this decrease in the size of ΔT_1, the steepness of the T_1-filter in the mD is increased and the amplification of contrast is increased. This maintains contrast as ΔT_1 and ΔTI decrease until the image becomes noise and/or artefact limited. Fourthly, Eq. (2) can be used to map T_1 in the mD since:

$$T_1 \approx \frac{\Delta TI}{\ln 4} S_{dSIR} + \frac{\Sigma TI}{\ln 4} \quad (3)$$

The linear approximation used in this section is only valid in the mD. Also, it is assumed that TR is long compared to tissue T_1 values, otherwise T_1 values may require correction for incomplete recovery of longitudinal magnetization during TR.

2.4 Summary of the Key Features of the dSIR Sequence

2.4.1 Contrast

The dSIR sequence can usefully increase contrast produced by small differences or changes in T_1 by ten or more times compared with conventional T_1-weighted IR sequences such as MP-RAGE.

The increase in contrast can be targeted at normal appearing white matter and can be achieved where it is particularly useful e.g., to improve visualization of subtle disease with small changes in T_1.

2.4.2 Boundaries

The dSIR sequence can show high signal, often high contrast boundaries between white and gray matter.

2.4.3 T_1 Maps

Because of the normalization of signals with dSIR images, ρ_m and T_2 effects are largely eliminated so dSIR images are essentially T_1 maps. There is a near linear relationship between signal and T_1 in the mD which can be used to provide direct reading of T_1 values in areas of interest on dSIR images.

3. Methods

With approval from the University of Auckland Hospital Research Ethics Committee (approval number AHRECAH1006), a 66-year-old female normal control and a 67-year-old female patient with a history of three episodes of mTBI over a 32 year period were scanned on a 3T scanner (SIGNA Premier; General Electric Healthcare, Milwaukee, WI) with an AIR™ 48-channel head coil. 2D FSE IR sequences were performed with a short TI_s to null normal white matter and a longer intermediate TI_i chosen to produce narrow mD dSIR images sensitive to small increases in T_1 from normal in white matter, as illustrated in Figure 4C. T_2-wSE and T_2-FLAIR images were acquired for comparison (Table 1).

Table 1 Pulse sequences and pulse sequence parameters used at 3T.

#	Sequence	TR (ms)	TI (ms)	TE (ms)	Matrix size Voxel sizes (mm)	Number of slices	Slice Thickness (mm)
1	2D FSE IR (for white matter nulling)	9,192	350	7	256 × 224 0.9 × 0.1 Z512 0.4 × 0.4	26	4
2	2D FSE IR (used with #1 for narrow mD dSIR)	5,796	500	7	256 × 224 0.9 × 0.1 Z512 0.4 × 0.4	26	4
3	2D T_2-wSE	2,200	-	102	300 × 280 0.8 × 0.9 Z512 0.5 × 0.5	26	4
4	3D T_2-FLAIR	6,300	1851	102	256 × 256 1 × 1 Z512 0.5 × 0.5	244	0.8

Z = zipped.

4. Results

4.1 Case History

The patient was a 67-year-old Asian woman who had sustained three mTBIs. She was married without children and has tertiary qualifications in early childhood education.

The first mTBI was in her mid-30s. She was a passenger in a motor vehicle crash when the car she was in slid underneath a truck. She recalls that she did not lose consciousness but was dazed for an unclear period following this. Her most prominent symptom was a problem with initiation of action, which was notably at variance with her premorbid character. This gradually improved with a return to her prior state although the time frame is unclear. She was able to quickly return to her employment as an early childhood education teacher.

The second injuring event occurred when she was 63 years old when she stood up underneath an open cupboard and struck her head. She was dazed but again did not lose consciousness. She was aware that she was more fatigued than usual and retired to bed at an earlier time than usual. She awoke the next morning more fatigued, with nausea and vomiting and collapsed. It is not clear if she lost consciousness but there is a period of about an hour that she has no recall of. She was aware of a sense of disorientation. She was taken to a local emergency service by ambulance where a diagnosis of concussion was made. After a period of observation she was sent home. She describes a developing head pain that encompassed her whole head and increased in severity with movement. Disequilibrium persisted. Nausea remained for a number of days. She was also having issues tolerating noise and light. Referral to a local Concussion Service resulted in a diagnosis of "typical concussion symptoms". There was a range of cognitive symptoms with slowed information processing, reaching cognitive overload more readily, difficulty in dividing and alternating attention with reduced attentional capacity and problems shifting mental set. She was more irritable. Physical issues included fatigue (particularly with mental effort), phonophobia, photophobia and persistent disequilibrium. Cervicogenic headache remained an ongoing issue. She engaged in a rehabilitation programme with the Concussion Service and started to return to work. Although there was a gradual reduction in symptom severity, she was not able to increase time at work beyond four hours per day.

The third injuring event was two years later. She was on an international flight and in standing up hit her head on the luggage compartment above her seat. There was an immediate onset of upper cervical pain, and pain radiating from the occiput to the vertex, associated with paraesthesia. There was an immediate slowing of information processing and she easily became cognitively overloaded. Attentional function worsened with further disruption in her capacity to divide and alternate attention, manage with an increased stimulus load and hold sufficient material in consciousness to allow sequencing of any behaviour that was not organizationally simple. She struggled with reading, having difficulty holding onto the plot, and tiring easily. Communication in any environment with other stimuli became difficult. She became much more irritable with her partner. Fatigue worsened to the extent that if overtired she was unable to sleep due to an inability to "switch off". As earlier, this arose especially with mental activity. Balance issues increased with a problem if she had to close her eyes in the shower. She described a sense of the ground moving underneath her. Thermoregulation issues arose with cold intolerance developing. There was also a a group of symptoms suggesting significant stressor effects, with ruminations, a default to presuming things were negative until proven otherwise, a lowered threshold for fight/flight reactivity and a reduction in positive hedonic response. Sense of taste and smell were unchanged from their premorbid state. Since then a standard multidisciplinary programme has led to only

limited improvement with much of this from the addition of methylphenidate which benefitted her attentional function. The results of MRI scanning are presented below.

4.2 MRI Findings

Figure 6 shows narrow mD 2D dSIR images acquired in the normal control and the patient. The control dSIR images showed white matter as low signal (dark) (left column). In the patient, the dSIR narrow mD images showed extensive high signal in white matter with only small areas of normal dark white matter in the anterior corpus callosum and peripheral white matter (right column, arrows). The control dSIR images show high signal, high contrast boundaries between white and gray matter. The boundaries are much less obvious in the patient images because of the high signal present in her abnormal white matter.

Figure 7 shows T_2-FLAIR and narrow mD dSIR images in the mTBI patient. Several small white matter hyperintensities are seen on T_2-FLAIR images (left column, short white arrows) but very extensive abnormalities with mild T_1 prolongation are seen in most of the white matter on the narrow mD dSIR images (right column). On the dSIR images, there are two areas of low signal (right column, long white arrows). These correspond to areas of increased signal on the T_2-FLAIR images (left column, short white arrows). They are due to large increases in T_2 and T_1. The large increase in T_1 results in lower signal intensity as shown by the blue curve in Figure 4C.

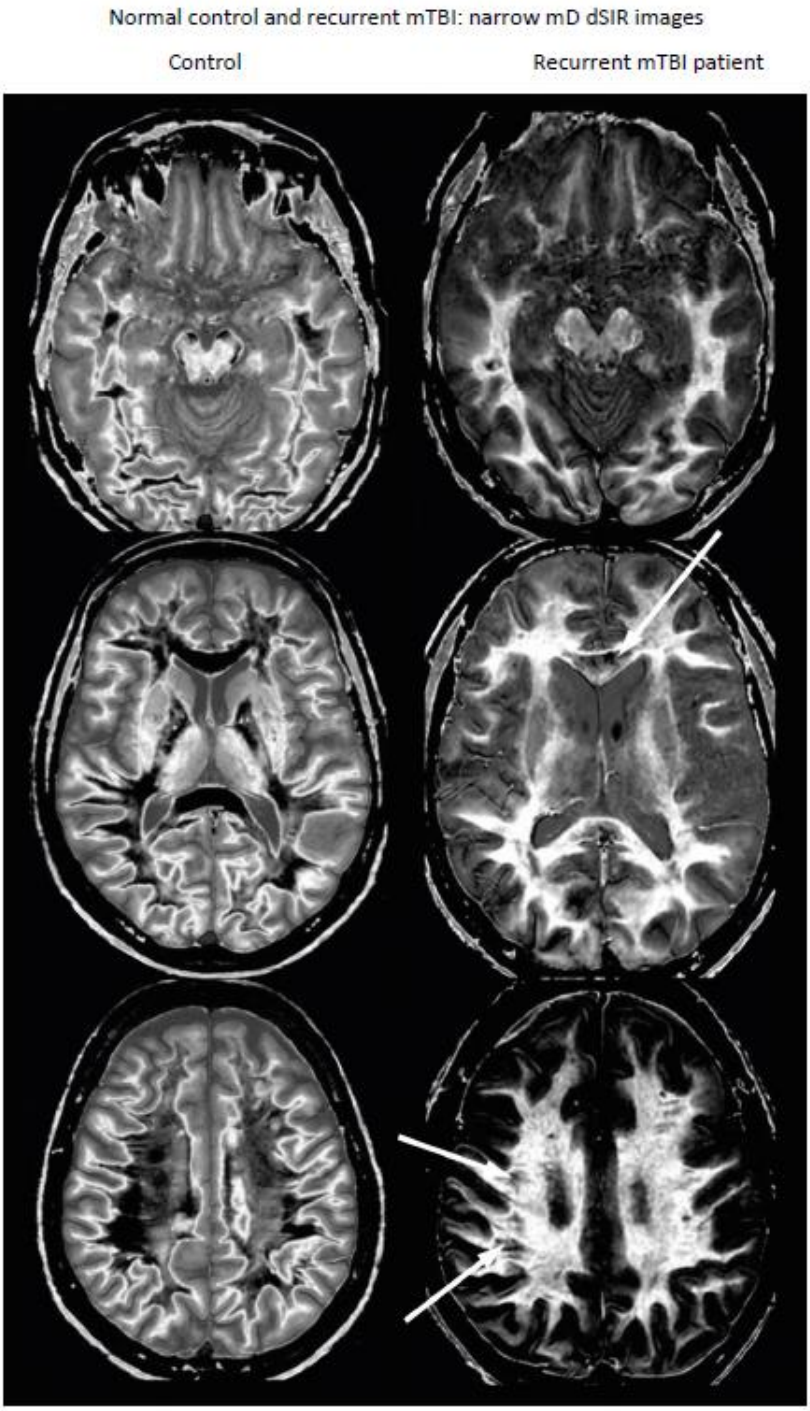

Figure 6 This shows 2D narrow mD dSIR images in the 66-year-old normal control (left column) and the 67-year-old patient with recurrent mTBI (right column). The dSIR narrow mD images on the control show normal white matter as very low signal intensity (dark) or mid gray e.g. the superior longitudinal fasciculi. The dSIR images on the mTBI patient show high signal changes in white matter which are very widespread. There are only small areas of normal dark white matter e.g., in the anterior corpus callosum and peripheral white matter (right column, white arrows). Normal high signal boundaries are seen between white and gray matter on the dSIR images of the control (left column) but are much more difficult to see in the patient (right column) because of the high signal present in her abnormal white matter.

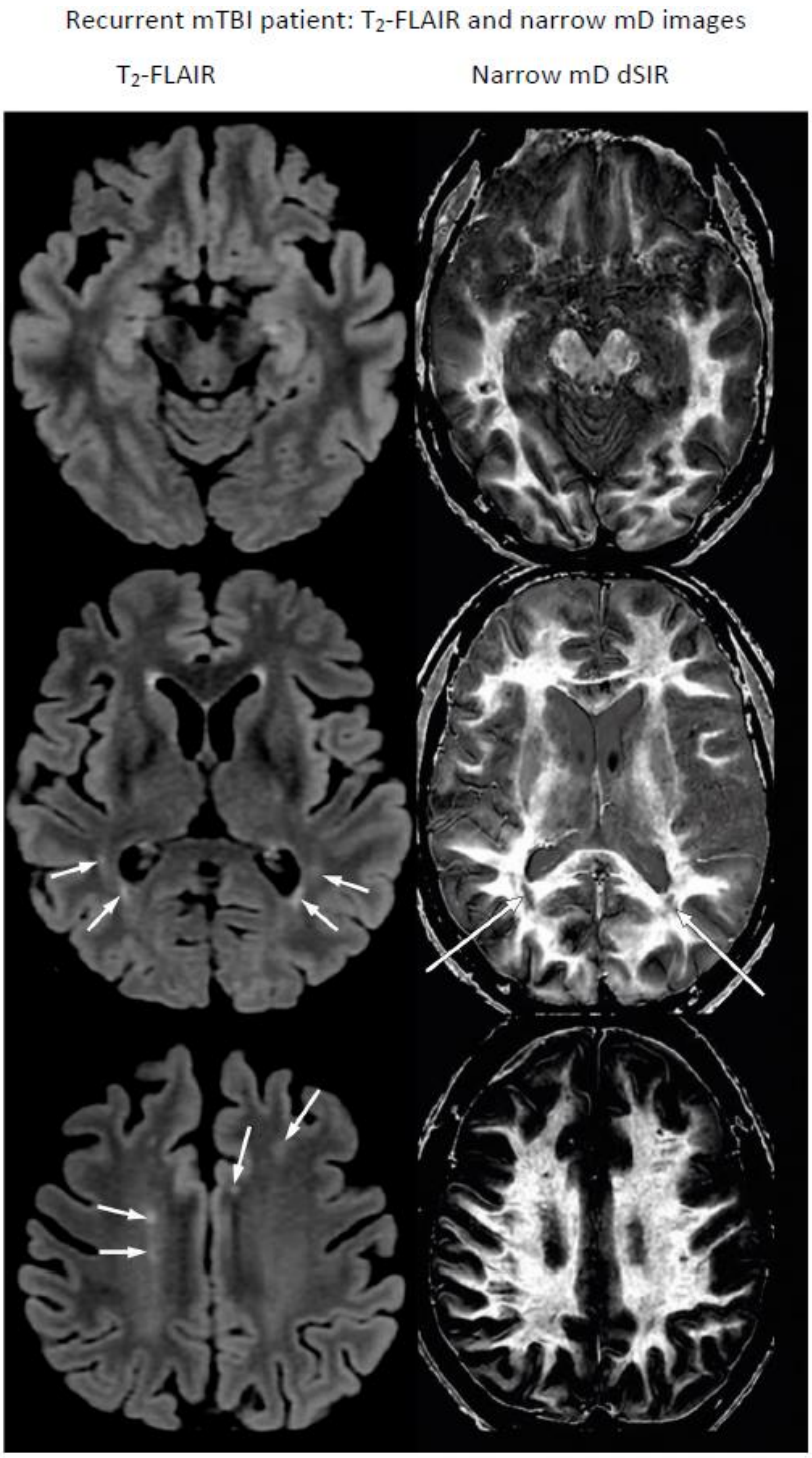

Figure 7 Comparison of T_2-FLAIR and narrow mD dSIR images in the patient with recurrent mTBI. Small areas of abnormality are seen on the T_2-FLAIR image (left column, white arrows) but there are very extensive areas of abnormal higher signal occupying about 90% of the white matter on the dSIR images (right column). There are low signal areas on the narrow mD dSIR images (right column, long white arrows) corresponding to high signal abnormal areas on the T_2-FLAIR images (left column, some short white arrows). These are a consequence of large increases in T_2 and T_1. The large increase in T_1 results in lower signal on the narrow mD dSIR image as shown by the blue curve in Figure 4C.

5. Discussion

This proof of principle study used a theoretical model of contrast involving a T_1-bipolar filter that predicted a large increase in contrast with dSIR sequences compared with conventional IR sequences. In a case of recurrent mTBI, very widespread abnormalities were seen in white matter that appeared normal, or showed only minor abnormalities, on T_2-FLAIR images.

5.1 Normal White Matter

Normal white matter may be subdivided into 20 or more categories [6]. It is very helpful to know the order of the T_1s of these normal tissues. Since dSIR images are T_1 maps, their signals in the mD can be linearly scaled to be T_1 values. As a result, the order of tissue signal or brightness directly follows their T_1 values. Nulling of white matter can be targeted at the white matter with the shortest T_1 of the relevant white matter tissues.

Identification of normal white matter is based on anatomical location, signal in relation to other normal white matter, symmetry, and studies of normal subjects of the same age with the same technique.

5.2 Normal Appearing White Matter

The term normal appearing white matter was first used in pathology and then applied to MRI in 1989 [7]. The term is used to describe white matter that appears normal with conventional T_1 and T_2-weighted sequences, but may be abnormal. The general approach used to detect such abnormalities has been to employ tissue properties other than T_1 and T_2 such as magnetization transfer, diffusion and metabolites such as N acetyl aspartate seen with MR spectroscopy.

In this paper, the approach to visualizing abnormalities in normal appearing white matter differs from the usual approach described above in that one of the same tissue properties used with conventional sequences is employed i.e., T_1. The argument is that changes in T_1 may be present in normal appearing white matter but these are too small to produce useful contrast with conventional sequences. To deal with this problem, a dSIR sequence producing ten or more times the contrast of conventional T_1-weighted IR sequences was used.

5.3 Targeting

All MRI examinations are targeted to a lesser or greater extent. Even whole body MRI includes sequences sensitive to only a few TPs. The term targeted MRI (tMRI) is usually applied to sequences specifically targeted at tissues, their TPs and/or changes in TPs in disease. dSIR employs more specific targeting than that of conventional m IR sequences which have a relatively broad T_1 domain of sensitivity to changes in T_1 as manifest by the slopes of their filters. They have a maximum slope centrally but lesser slopes reaching flat plateaus at low and high values of T_1 where they are less sensitive to changes in T_1 (e.g., Figure 1B). dSIR sequences have a much narrower mD where they are particularly sensitive to changes in T_1. The contrast dSIR sequences produce from small changes in T_1 in this narrow mD is far greater than that produced by conventional m IR sequences (Figure 4C).

5.4 dSIR T_1-bipolar Filters

dSIR T_1-bipolar filters provide a valuable means of understanding the targeting, contrast, boundaries, and T_1 mapping seen with dSIR sequences. dSIR sequences are univariate for T_1 (i.e., dependent on T_1 but not on ρ_m or T_2) and are comprehensive i.e., only a T_1 TP-filter is needed to interpret dSIR images, unlike for example SE, STIR and T_2-FLAIR images where three different TP-filters (ρ_m, T_1 and T_2) are necessary to understand them.

As ΔTI becomes smaller, the small change approximation of differential calculus used for TP-filters, and the linear approximation used for T_1 mapping both become more accurate.

5.5 Technical Features

The sequences used to create dSIR images (2D IR Fast Spin Echo [FSE], 3D IR Gradient Echo [GE]) are widely available on standard MRI systems and usually require no special implementation.

The coding required to add, subtract and divide IR images can written in MATLAB or other similar packages. Rigid body registration packages are widely available e.g., in FSL (fMRIB software library) to re-align misregistered images.

Acquisitions can be shortened by interleaving the two different TI acquisitions in a single sequence. There are also likely to be benefits in scan time by use of parallel imaging, compressed sense and deep learning reconstruction algorithms.

5.6 Neuroinflammation and Neurodegeneration

Neuroinflammation has long been regarded as a mechanism underpinning multiple sclerosis and other diseases of white matter [2-8]. It is also thought to be a critical mechanism in traumatic brain injury [9-11]. Neuroinflammation may be associated with or precede neurodegeneration. These pathological processes may account for the widespread small increases in T_1 seen in the white matter of the patient with recurrent mTBI.

5.7 Limitations

High contrast images resulting from small changes in T_1 are strictly only available for T_1 changes within the mD. As can be seen from the T_1-bipolar filter, contrast is rapidly lost for values of T_1 outside of the mD. If the mD is too narrow, then changes in T_1 can result in a lesion moving rightward on the filter onto the negatively sloped or flat part of the curve. This limits how bright a lesion appears and T_1 mapping will be inaccurate. However, the lesion will have a high signal boundary and be visible.

dSIR images are complementary to conventional images which are less sensitive to changes in T_1 but cover a wider domain of T_1 values.

Targeting requires selection of the baseline or nulling T_1 for white matter as well as the sign and size of changes in T_1 from the normal values in disease. It is possible to use multiple TIs to cover more options for normal values and changes in T_1.

It is also possible to produce a T_1 map with techniques such as magnetic resonance fingerprinting, synthetic MRI and Magnetization Prepared 2 Rapid Acquisition Gradient Echo (MP2RAGE), and use these T_1 maps to construct synthetic dSIR images. From a single T_1 map, multiple dSIR images can be produced with varying TIs and mDs.

6. Conclusions

dSIR sequences targeted at small increases in T_1 in white matter showed extensive high contrast abnormalities in areas of white matter that appeared normal using T_2-wSE and T_2-FLAIR sequences in a patient with recurrent mTBI. The approach may have wide application for detecting subtle abnormalities in white matter in TBI and other diseases.

Abbreviations

AIR	Added IR
dSIR	divided Subtracted Inversion Recovery
FSE	Fast Spin Echo
FSL	FMRIB Software Library
FMRIB	Functional MRI of the Brain
G	Gray matter
IR	Inversion Recovery
TI	Inversion Time
TI_i	Inversion Time intermediate
TI_l	Inversion Time long
TI_s	Inversion Time short
MRI	Magnetic Resonance Imaging
MP-RAGE	Magnetization Prepared Rapid-Acquisition Gradient Echo
MP2RAGE	Magnetization Prepared 2 Rapid Acquisition Gradient Echo
m	magnitude
mD	middle Domain
mTBI	mild Traumatic Brain Injury
ps	phase-sensitive
TR	Repetition Time
STIR	Short TI IR
SE	Spin Echo
SIR	Subtracted Inversion Recovery
T_2-wSE	T_2-weighted Spin Echo
T_2-FLAIR	T_2- FLuid Attenuated Inversion Recovery
tMRI	targeted MRI
3D	Three Dimensional
TP	Tissue Property
2D	Two dimensional
W	White matter
Z	Zipped

Author Contributions

(I) Conception and design: All authors; (II) Administrative support: GN, SJH; (III) Provision of study materials or patients: GN, PC, DMC; (IV) Collection and assembly of data: GN, PC; (V) Data analysis

and interpretation: JPM, EEK, DMC; (VI) Manuscript writing: All authors; (VII) Final approval of manuscript: All authors.

Funding

We would like to acknowledge support from the Fred Lewis Enterprise Foundation, the Hugh Green Foundation, anonymous donor, the JN &HB Williams Foundation, Mangatawa Beale Williams Memorial Trust, and Kānoa New Zealand. We are also grateful for support from GE Healthcare and Mātai Ngā Māngai Māori.

Competing Interests

All authors have completed the ICMJE uniform disclosure form (available at http://dx.doi.org/10.21037/qims.2020.04.07). GMB is a clinical consultant to Magnetica, Brisbane, Australia. The other authors have no conflicts of interest to declare.

References

1. Maas AI, Menon DK, Adelson PD, Andelic N, Bell MJ, Belli A, et al. Traumatic brain injury: Integrated approaches to improve prevention, clinical care, and research. Lancet Neurol. 2017; 16: 987-1048.
2. Schimmel SJ, Acosta S, Lozano D. Neuroinflammation in traumatic brain injury: A chronic response to an acute injury. Brain Circ. 2017; 3: 135-142.
3. Zheng RZ, Lee KY, Qi ZX, Wang Z, Xu ZY, Wu XH, et al. Neuroinflammation following traumatic brain injury: Take it seriously or not. Front Immunol. 2022; 13: 855701.
4. Maas AI, Menon DK, Manley GT, Abrams M, Åkerlund C, Andelic N, et al. Traumatic brain injury: Progress and challenges in prevention, clinical care, and research. Lancet Neurol. 2022; 21: 1004-1060.
5. Ma YJ, Moazamian D, Cornfeld DM, Condron P, Holdsworth SJ, Bydder M, et al. Improving the understanding and performance of clinical MRI using tissue property filters and the central contrast theorem, MASDIR pulse sequences and synergistic contrast MRI. Quant Imaging Med Surg. 2022; 12: 4658-4690.
6. Bullock DN, Hayday EA, Grier MD, Tang W, Pestilli F, Heilbronner SR. A taxonomy of the brain's white matter: Twenty-one major tracts for the 21st century. Cereb Cortex. 2022; 32: 4524-4548.
7. Kesselring J, Miller DH, MacManus DG, Johnson G, Milligan NM, Scolding N, et al. Quantitative magnetic resonance in multiple sclerosis: The effect of high dose intravenous methylprednisolone. J Neurol Neurosurg Psychiatry. 1989; 52: 14-17.
8. Graham NS, Sharp DJ. Understanding neurodegeneration after traumatic brain injury: From mechanisms to clinical trials in dementia. J Neurol Neurosurg Psychiatry. 2019; 90: 1221-1233.
9. Anzai Y, Minoshima S. Imaging of traumatic brain injury: Current and future. Imaging Med. 2011; 3: 153-165.
10. Asken BM, Rabinovici GD. Identifying degenerative effects of repetitive head trauma with neuroimaging: A clinically-oriented review. Acta Neuropathol Commun. 2021; 9: 96.
11. Koerte IK, Lin AP, Willems A, Muehlmann M, Hufschmidt J, Coleman MJ, et al. A review of neuroimaging findings in repetitive brain trauma. Brain Pathol. 2015; 25: 318-349.